Imaging of alkyne-functionalized ruthenium complexes for photoactivated chemotherapy

Busemann, A.

3

RUTHENIUM-BASED PACT AGENTS: SYNTHESIS, PHOTOCHEMISTRY, AND CYTOTOXICITY STUDIES

*The series of complexes [Ru(tpy)(NN)(Hmte)]$(PF_6)_2$, where tpy = 2,2′:6′,2″-terpyridine, NN = 2,2′-bipyridine (bpy, **[1]**$(PF_6)_2$), 3,3′-biisoquinoline (i-biq, **[2]**$(PF_6)_2$), or di(isoquinolin-3-yl)amine (i-Hdiqa, **[3]**$(PF_6)_2$), and Hmte = 2-(methylthio)ethanol, were synthesized and their photochemical and (photo)cytotoxic properties were investigated in order to assess their suitability as photoactivated chemotherapy (PACT) agents. The increase of the aromatic surface of **[2]**$(PF_6)_2$ and **[3]**$(PF_6)_2$, compared to **[1]**$(PF_6)_2$, leads to higher lipophilicity and higher cell uptake for the former complexes. Such improved uptake is directly correlated to the cytotoxicity of these compounds in the dark: while **[2]**$(PF_6)_2$ and **[3]**$(PF_6)_2$ showed low EC_{50} values in human cancer cells, **[1]**$(PF_6)_2$ is not cytotoxic due to poor cellular uptake. While stable in the dark, all complexes substituted the protecting thioether ligand upon light irradiation (520 nm), with the highest photosubstitution quantum yield found for **[3]**$(PF_6)_2$ ($\Phi_{[3]}$ = 0.070). Compounds **[2]**$(PF_6)_2$ and **[3]**$(PF_6)_2$ were found both more cytotoxic after light activation than in the dark, with a photo index of 4. Considering the very low singlet oxygen quantum yields of these compounds, and the lack of cytotoxicity of the photoreleased Hmte thioether ligand, it can be concluded that the toxicity observed after light activation is due to the photoreleased aqua complexes $[Ru(tpy)(NN)(OH_2)]^{2+}$, and thus that **[2]**$(PF_6)_2$ and **[3]**$(PF_6)_2$ are promising PACT candidates.*

3.1 Introduction

In recent years, ruthenium polypyridyl complexes gained attention in the field of phototherapy for their favorable photophysical and photochemical properties.[1] Drug activation by light irradiation at the tumor site provides physical selectivity towards cancerous tissues and minimizes the effect of the drug on the healthy, non-irradiated tissues. Therefore, undesired side effects are expected to be reduced. Two different types of phototherapy are distinguished: photodynamic therapy (PDT) and photoactivated chemotherapy (PACT). In both cases, a molecule is promoted to a singlet metal-to-ligand charge transfer excited state (^{1}MLCT) by photon absorption. From there, the molecule undergoes intersystem crossing (ISC) to a triplet metal-to-ligand charge transfer excited state (^{3}MLCT). This ^{3}MLCT state can be deactivated *via* four different pathways: non-radiative deactivation, emission of a photon, energy transfer to molecular oxygen to generate singlet oxygen ($^1O_2$), or thermal population of a low-lying triplet metal-centered excited state (^{3}MC), which leads to ligand photosubstitution. In PDT, the production of $^1O_2$ leads to serious oxidative damage of the cells, culminating in cell death. In PACT, on the other hand, the prodrug, which is usually poorly toxic in the dark, is activated by ligand photosubstitution. The activated drug becomes capable of interacting with biomolecules, causing cell death in an oxygen-independent way.[2-5] Since thermal promotion from the photochemically generated ^{3}MLCT state into the photosubstitutionally active ^{3}MC state is a competitive pathway for the quenching of the ^{3}MLCT state, good PACT agents are usually not emissive and produce only small amounts of $^1O_2$.

In order to be a promising PACT agent, a metal complex has to fulfill three criteria: i) it should be thermally stable in solution in the dark, ii) it should be photoactivatable with acceptable photosubstitution quantum yields, typically in the order of $\Phi \sim 0.01 - 0.05$, and iii) it should show an increased cytotoxicity after light activation, compared to the dark. For example, [Ru(tpy)(bpy)(Hmte)](PF$_6$)$_2$ ([**1**](PF$_6$)$_2$, where tpy = 2,2′:6′,2″-terpyridine, bpy = 2,2′-bipyridine, and Hmte = 2-(methylthio)ethanol), is known to undergo photosubstitution under blue light irradiation.[6] Although its cytotoxic properties have not been reported yet, its activated aqua photoproduct [Ru(tpy)(bpy)(OH$_2$)]$^{2+}$ is known to be non-cytotoxic.[7] To obtain high cytotoxicity, ruthenium complexes require efficient cellular uptake and interaction of the activated metal complex with biological molecules. Bicationic ruthenium complexes often show low cellular uptake.[8] This issue, however, can be solved either by

lowering the positive charge of the complex, *e.g. via* cyclometallation,[9, 10] or by increasing the hydrophobicity of the ligands, *e.g.* by expanding the aromatic surface of a polypyridyl ligand or by adding methyl groups.[11, 12] On the other hand, too lipophilic complexes often show too high dark cytotoxicity, which is a problem in phototherapy.[13] For PACT compounds, ligand expansion aimed at increasing steric hindrance and thus photosubstitution efficacy,[14, 15] may also lead to too distorted complex geometries, resulting in uncontrolled ligand release and thermal activation in the dark.[6, 12, 16] Overall, the design of a good PACT compound requires careful balancing of the lipophilicity of the complex and its photoreactivity altogether.

In this work, two new ruthenium-based PACT compounds with the formula [Ru(tpy)(NN)(Hmte)]$(PF_6)_2$ (where NN = i-biq (3,3'-biisoquinoline), [**2**]$(PF_6)_2$; or i-Hdiqa (di(isoquinolin-3-yl)amine), [**3**]$(PF_6)_2$); Figure 3.1), are reported. The increased aromatic surface of the bidentate ligands, compared to bpy, is expected to improve the cellular uptake. In addition, the dipyridylamine (Hdpa) scaffold, on which i-Hdiqa is based, is known to play a role in cellular uptake, compared to bpy-based systems.[17] Considering the promising results obtained with the tetrapyridyl complex $[Ru(H_2biqbpy)(dmso)(Cl)]^+$, where $H_2biqbpy$ = 6,6′-bis[*N*-(isoquinolyl)-1-amino]-2,2′-bipyridine,[18] an amine bridge is introduced to the i-biq ligand resulting in the i-Hdiqa analogue, thus extending the family of $[Ru(tpy)(NN)(SRR')]^{2+}$ complexes, which has been studied extensively.[19] Next to cellular uptake, the enlarged aromatic rings of the ligands i-biq and i-Hdiqa may also enhance intercalation of the complex with proteins, membranes, or DNA, which may lead to improved cytotoxicity.[20] The monodentate thioether ligand Hmte, on the other hand, provides excellent thermal stability in the dark, while offering good photochemical release.[6] The synthesis, photochemistry, cytotoxicity, and cellular uptake of these compounds are reported, and compared to that of the known complex [**1**]$(PF_6)_2$.

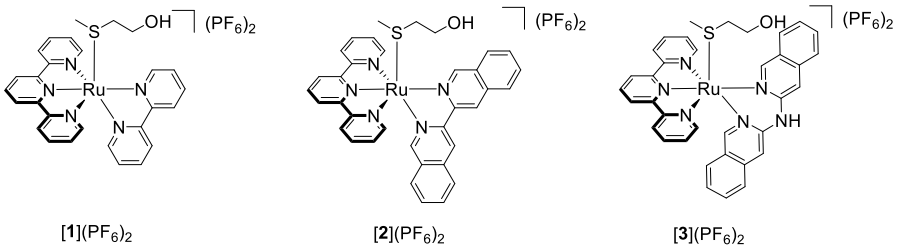

[**1**]$(PF_6)_2$ [**2**]$(PF_6)_2$ [**3**]$(PF_6)_2$

Figure 3.1. Chemical structures of the ruthenium-based PACT agents [**1**]$(PF_6)_2$ – [**3**]$(PF_6)_2$.

3.2 Results and Discussion

3.2.1 Synthesis and Characterization

The bidentate ligand i-biq was obtained following a reported procedure.[21] The ligand i-Hdiqa was synthesized using a Buchwald-Hartwig coupling and purified by column chromatography. The two ruthenium-based PACT compounds [**2**](PF$_6$)$_2$ and [**3**](PF$_6$)$_2$ were synthesized following the same reaction route as for [**1**](PF$_6$)$_2$ (Scheme AIII.1). In short, the bidentate ligand was first coordinated to the ruthenium precursor [Ru(tpy)(Cl)$_3$], before the monodentate chloride ligand was thermally substituted by the protecting thioether ligand Hmte. The desired complexes were obtained in good yield (50 and 60%, respectively), and their purity was confirmed with ^{1}H NMR, ^{13}C NMR, and elemental analysis.

Single crystals suitable for X-ray structure determination of complex [**2**](PF$_6$)$_2$ were obtained in the dark by slow vapor diffusion of diisopropyl ether in an acetonitrile solution of the complex (Figure 3.2). Selected bond lengths, angles, and torsion angles are summarized in Table 3.1 and are compared to those of [**1**](PF$_6$)$_2$.[6] The coordination bond lengths of the i-biq complex are not significantly different from those with bpy *e.g.* Ru-N4 is 2.104(10) *vs.* 2.092(1) Å for [**2**](PF$_6$)$_2$ *vs.* [**1**](PF$_6$)$_2$. The torsion angle of the coordinated i-biq is slightly smaller than that of bpy (N4-C24-C25-N5 = 1.9(14)° *vs.* N4-C20-C21-N5 = 5.3(2)°, Table 3.1). The Hmte ligand is bound *via* the sulfur atom to ruthenium, with similar bond lengths for both complexes (Ru-S = 2.368(3) and 2.3690(5) for [**2**](PF$_6$)$_2$ and [**1**](PF$_6$)$_2$, respectively). As single crystals for complex [**3**](PF$_6$)$_2$ could not be obtained, density functional theory (DFT) was used to compare the structure of [**3**]$^{2+}$ (Figure 3.2) to that of [**2**]$^{2+}$ (Table AIII.2 and AIII.3). The bond distances and angles of the DFT models of [**2**]$^{2+}$ and [**3**]$^{2+}$ are also provided in Table 3.1. For [**2**]$^{2+}$, the minimized geometry of the DFT model was very close to that of the X-ray structure. For [**3**]$^{2+}$, no significant differences in bond lengths or angles are found compared to [**2**]$^{2+}$, however, the position of the bidentate ligand towards the tpy ligand does differ. While i-biq is perpendicular to the tpy ligand, i-Hdiqa shows a characteristic bending at the amine bridge (Figure AIII.10).[22, 23] Calculations of the bond angle variance (σ^2 = 60.3 and 46.4, respectively),[24] and the mean quadratic elongation (λ = 3.65 and 3.46, respectively),[25] revealed that the octahedral geometry of both complexes is distorted, but that this distortion is mostly caused by the coordination of the tpy ligand (N1-Ru1-N3 = 158.17 and 158.01°, respectively). Overall, the extension of the bpy ligand into i-biq

or i-Hdiqa does not lead to significant changes of the coordination sphere or bond lengths to the ruthenium ion.

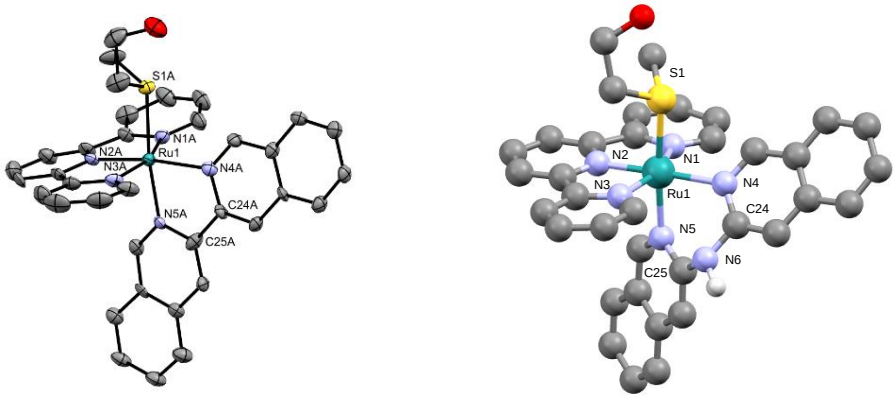

Figure 3.2. Displacement ellipsoid (50% probability level) of one crystallographically independent cationic part as observed in the crystal structure of $[\mathbf{2}]^{2+}$ (left). The other cation, disorder, counter ions, and H atoms have been omitted for clarity. DFT-minimized structure of $[\mathbf{3}]^{2+}$ (right).

Table 3.1. Selected bond lengths (Å), angles (°), and torsion angles (°) for [**1**](PF$_6$)$_2$ – [**3**](PF$_6$)$_2$.

	[1](PF$_6$)$_2$ [a]	**[2](PF$_6$)$_2$** [b]	**[2]$^{2+}$** [c]	**[3]$^{2+}$** [c]
Ru-N1	2.061(1)	2.071(9)	2.094	2.095
Ru-N2	1.961(1)	1.967(10)	1.979	1.978
Ru-N3	2.066(1)	2.073(10)	2.096	2.114
Ru-N4	2.092(1)	2.104(10)	2.117	2.138
Ru-N5	2.064(1)	2.074(9)	2.082	2.115
Ru-S1	2.3690(5)	2.368(3)	2.396	2.396
N1-Ru1-N2	80.08(6)	79.3(4)	79.14	79.17
N2-Ru1-N3	79.39(6)	80.1(4)	79.19	78.90
N1-Ru1-N3	159.31(6)	159.4(4)	158.17	158.01
N4-Ru1-N5	78.12(6)	79.4(4)	78.43	86.45
N4-C20-C21-N5	5.3(2)	—	—	—
N4-C24-C25-N5	—	1.9(14)	4.46	—
λ [d]			3.65	3.46
σ^2 [e]			60.3	46.4

[a] data from Bahreman *et al.*;[6] [b] data obtained by X-ray analysis (provided only for the crystallographically independent cation labelled A in the asymmetric unit of [**2**](PF$_6$)$_2$); [c] data from DFT calculations at the PBE0/TZP/COSMO level in water. [d] $\lambda = \frac{1}{6}\sum_{n=1,6}\left[\frac{d_n - <d>}{<d>}\right]^2$, mean quadratic elongation, where d_n is one of the six bond lengths and <d> is the mean of those bond lengths; [e] $\sigma^2 = \frac{1}{11}\sum_{n=1,12}(\theta_n - 90)^2$, bond angle variance where θ_n is one of the twelve angles.

3.2.2 Photochemistry

Compounds [**2**](PF$_6$)$_2$ and [**3**](PF$_6$)$_2$ are thermally stable in water in the dark at 37 °C for 24 h (Figure AIII.1a and b). The two complexes have an ^{1}MLCT absorption band at 429 and 470 nm for [**2**]$^{2+}$ and [**3**]$^{2+}$, respectively, with similar molar absorption coefficients (Table 3.2, Figure AIII.2). Compared to [**1**](PF$_6$)$_2$, the ^{1}MLCT state of i-biq-based [**2**](PF$_6$)$_2$ is shifted to lower wavelengths, while i-Hdiqa-based [**3**](PF$_6$)$_2$ shows a bathochromic shift, caused by a lower π orbital overlap due to the bending of the i-Hdiqa ligand. Phosphorescence measurements upon irradiation of the complexes with blue light (450 nm) in deuterated methanol showed that phosphorescence quantum yields Φ_P are lower than $5 \cdot 10^{-4}$ for all three complexes. In addition, the complexes show only very low singlet oxygen quantum yields Φ_Δ, confirming that they are not suitable as PDT agents (Table 3.2 and Figure AIII.3).

Table 3.2. Lowest-energy absorption maxima (λ_{max} in nm), molar absorption coefficients at λ_{max} (ε_{max} in $M^{-1} \cdot cm^{-1}$) in water, singlet oxygen generation quantum yields (Φ_Δ) in aerated methanol-d_4, phosphorescence quantum yields (Φ_P) in aerated methanol-d_4, and photosubstitution quantum yields upon irradiation at 517 nm (Φ_{517}) in water for complexes [**1**]$(PF_6)_2$ – [**3**]$(PF_6)_2$.

complex	NN	λ_{max} (ε_{max}) [a]	Φ_P [b]	Φ_Δ [b]	Φ_{517} [a]
[**1**]$(PF_6)_2$	bpy	450 ($6.60 \cdot 10^3$) [c]	$< 1.0 \cdot 10^{-4}$ [d]	< 0.005 [d]	0.022 [c]
[**2**]$(PF_6)_2$	i-biq	429 ($5.76 \cdot 10^3$)	$1.5 \cdot 10^{-4}$	0.010	0.023
[**3**]$(PF_6)_2$	i-Hdiqa	470 ($5.35 \cdot 10^3$)	$4.5 \cdot 10^{-4}$	0.042	0.077

[a] in water; [b] in methanol-d_4;[26] [c] data taken from Bahreman *et al.*;[6] [d] data from Chapter 2.

The photoreactivities of [**2**]$(PF_6)_2$ and [**3**]$(PF_6)_2$ upon green light irradiation (517 nm) in water at 37 °C were investigated using UV-vis spectroscopy (Figure 3.3). For each complex, upon irradiation a typical bathochromic shift of the absorption maximum was observed, due to the release of the thioether ligand and the formation of the corresponding aqua complex $[Ru(tpy)(NN)(OH_2)]^{2+}$ ([**4**]$^{2+}$ and [**5**]$^{2+}$ for NN = i-biq and i-Hdiqa, respectively, see Scheme 3.1).[19, 27, 28] The formation of the aqua complexes was confirmed with mass spectrometry (Figure AIII.4). The UV-vis spectra recorded during irradiation showed isosbestic points (at 369; 375 and 404, respectively), indicating a one-step photosubstitution reaction. The Glotaran software package was used to fit the time evolution of the UV-vis absorption spectra to a single photoreaction, and to obtain the photosubstitution quantum yields Φ_{517} (Table 3.2, Figure AIII.5).[29] The quantum yields of [**1**]$(PF_6)_2$ and [**2**]$(PF_6)_2$ were found similar (Φ_{517} = 0.022 and 0.023 for [**1**]$^{2+}$ and [**2**]$^{2+}$, respectively). Thus, changing the bidentate ligand from bpy to i-biq does not alter the photosubstitution efficacy. However, the presence of i-Hdiqa in [**3**]$^{2+}$ increased the quantum yield by 3.5-fold (Φ_{517} = 0.077). The reason for the increased photosubstitution quantum yield of the Hmte ligand in [**3**]$^{2+}$ remains unclear. Overall, efficient quenching of the ^{3}MLCT state by population of the ^{3}MC state results for both complexes in non-emissive compounds with very low singlet oxygen production, and with significant to high photosubstitution quantum yields. Therefore, complexes [**2**]$(PF_6)_2$ and [**3**]$(PF_6)_2$ fulfill the photochemical criteria of potential PACT candidates.

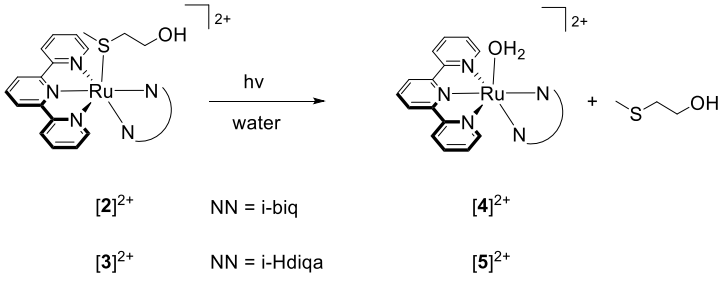

Scheme 3.1. Photosubstitution of the protecting Hmte ligand in $[Ru(tpy)(NN)(Hmte)]^{2+}$ ($[\mathbf{2}]^{2+}$ and $[\mathbf{3}]^{2+}$) to form the corresponding aqua species $[Ru(tpy)(NN)(OH_2)]^{2+}$ ($[\mathbf{4}]^{2+}$ and $[\mathbf{5}]^{2+}$).

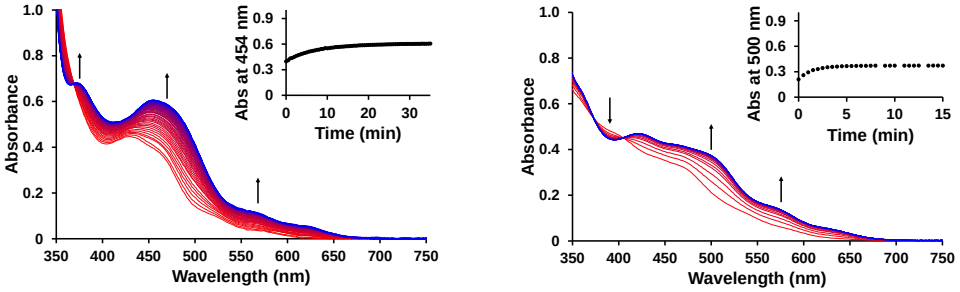

Figure 3.3. Evolution of the UV-vis absorption spectra of a solution of $[\mathbf{2}](PF_6)_2$ (left) and $[\mathbf{3}](PF_6)_2$ (right) upon green light irradiation in water. Conditions: [Ru] = 0.074 and 0.061 mM for $[\mathbf{2}](PF_6)_2$ and $[\mathbf{3}](PF_6)_2$, respectively, T = 37 °C, light source: λ = 517 nm, $\Delta\lambda_{1/2}$ = 23 nm, 5.2 mW, photon flux $\Phi = 5.2 \cdot 10^{-8}$ mol · s^{-1} for $[\mathbf{2}](PF_6)_2$ and $[\mathbf{3}](PF_6)_2$, V = 3 mL, under air atmosphere. Inset: Time evolution of absorbance at wavelength 454 nm for $[\mathbf{2}](PF_6)_2$ and 500 nm for $[\mathbf{3}](PF_6)_2$.

3.2.3 Cytotoxicity and cellular uptake

For PACT agents, dark stability under cell growing conditions is essential, so the thermal stability of all complexes was also studied with UV-vis spectroscopy in cell medium (OptiMEM complete) at 37 °C (Figure AIII.1c and d). All complexes were found to be stable for at least 24 h under such conditions. Then, the cytotoxicity of complexes $[\mathbf{1}](PF_6)_2$ – $[\mathbf{3}](PF_6)_2$ was tested under normoxic conditions (21% O_2) in 2D monolayers of human lung carcinoma (A549) and human epidermoid carcinoma (A431) cell lines, following a protocol developed by Hopkins *et al.*[30] In short, cancer cells were seeded at t = 0 h, treated with six different complex concentrations at t = 24 h, and irradiated at t = 48 h with the light of a green LED for 30 min (520 nm, 38 J/cm^2). The irradiation time, necessary to fully activate the complexes, was determined using UV-vis spectroscopy (Appendix 1 and Figure AIII.6). At t = 96 h a Sulforhodamine B (SRB) assay was performed to compare the cell viability in treated *vs.* untreated cells (Figure AIII.7 and AIII.8). The effective concentrations (EC_{50} values), *i.e.* the concentration at which the cell viability was reduced by 50%

compared to untreated cells, are reported in Table 3.3. The photo index of each compound was calculated as the ratio of the EC_{50} values obtained in the dark and upon light irradiation.

The bpy-based complex [**1**]$(PF_6)_2$ was found to be non-cytotoxic against A549 cancer cells, whether irradiated or not (EC_{50} > 150 μM, Figure AIII.9). The complexes [**2**]$(PF_6)_2$ and [**3**]$(PF_6)_2$ showed low cytotoxicity in the dark (80 *vs.* 62 μM), but revealed a significant increase in cytotoxicity after light activation characterized by EC_{50} values of 21 and 14 μM, respectively. These changes correspond to photo indices of ~ 4 for both complexes, indicating that a more cytotoxic species is released upon light activation. The released thioether ligand Hmte, tested independently, showed neither cytotoxicity in the dark nor upon light irradiation. Therefore, the cytotoxicity observed upon light irradiation of $[\mathbf{2}]^{2+}$ or $[\mathbf{3}]^{2+}$ must be based on the metal-containing photoproduct, *i.e.* the aqua complexes $[\mathbf{5}]^{2+}$ and $[\mathbf{6}]^{2+}$, respectively.[31, 32] In A431 cancer cells, the same trends were observed (Table 3.3). Cytotoxicity experiments under hypoxic conditions (1% O_2) need to be undertaken for complexes [**2**]$(PF_6)_2$ and [**3**]$(PF_6)_2$ to confirm whether they remain phototoxic also at low oxygen levels, as true PACT agents should.

Table 3.3. (Photo)cytotoxicity (EC_{50} with 95% confidence interval in μM) of [**1**]$(PF_6)_2$, [**2**]$(PF_6)_2$, [**3**]$(PF_6)_2$, and Hmte in lung cancer cells (A549) and skin cancer cells (A431) under normoxic conditions (21% O_2).[a] Cellular uptake (CU in nmol Ru/ mg cell protein) of [**1**]$(PF_6)_2$ – [**3**]$(PF_6)_2$ in lung cancer cells (A549) under normoxic conditions (21%).[b]

		[1](PF6)2	[2](PF6)2		[3](PF6)2		Hmte
A549	dark	>150	79.7	+6.1 −5.7	62.1	+16.4 −13.8	>150
	light	>150	20.6	+3.0 −2.6	13.8	+4.3 −3.6	>150
	PI [c]	—	3.9		4.5		—
	CU	0.16 ± 0.11	0.32 ± 0.14		0.69 ± 0.16		—
A431	dark	>150	55.2	+7.5 −6.5	42.9	+9.2 −7.5	>150
	light	>150	12.2	+1.5 −1.4	11.2	+2.7 −2.4	>150
	PI [c]	—	4.5		3.8		—

[a] Cytotoxicity experiments were performed in biological and technical triplicate; [b] Results of cellular uptake experiments upon incubation for 24 h with 30 μM drug in the dark. Experiments were performed in biological triplicate; [c] photo index (PI) is defined as $EC_{50,\,dark}$/ $EC_{50,\,light}$.

To quantify the effect of the increased hydrophilicity of the complexes, by extending the aromaticity of the ligands, on the cellular uptake, uptake experiments were performed. A549 cells were treated with 30 μM of the complex, which is lower than the EC_{50} values, and the uptake was determined after 24 h incubation in the dark (Table 3.3). The ruthenium content in nmol per mg cell protein was determined by high-resolution continuum-source atomic absorption spectrometry (HRCS AAS, further details in Appendix 1) under normoxic (21% O_2). Complex [**1**]$(PF_6)_2$ was very poorly taken up (0.16 nmol per mg cell protein), which explains its lack of cytotoxicity against cancer cells. For the other two complexes, the ruthenium uptake was higher, *i.e.* 0.32 and 0.69 nmol per mg cell protein, respectively, under normoxic conditions. According to these results, dipyridylamine-based ligands such as i-Hdiqa enhance complex accumulation compared to their bpy analogues (here i-biq).[17]

3.3 Conclusions

The known photoactivatable ruthenium complex [**1**]$(PF_6)_2$ is very poorly taken up by cells and as a result shows no (photo)cytotoxicity. Therefore, it is not suitable as a

PACT agent. However, two analogue ruthenium complexes with more hydrophobic bidentate ligands were shown to be promising PACT compounds. Complex [**2**]$(PF_6)_2$ shows comparable photochemical properties as [**1**]$(PF_6)_2$, but the higher lipophilicity significantly increases cellular uptake. This allows the photosubstitution reaction to occur inside the cell and to result into increased cytotoxicity upon green light irradiation. [**3**]$(PF_6)_2$, which has an additional non-coordinated amine bridge, shows an enhanced photosubstitution quantum yield compared to $[\mathbf{2}]^{2+}$ and enhanced cellular uptake, but it has a similar photo index compared to $[\mathbf{2}]^{2+}$. Cytotoxicity studies under hypoxic conditions need to be undertaken with [**2**]$(PF_6)_2$ and [**3**]$(PF_6)_2$ to investigate whether the oxygen-independent activation mechanism translates into interesting biological photoactivation also in hypoxic cancer cells.

3.4 Experimental

3.4.1 Methods and Materials

$RuCl_3$ was purchased from Alfa Aesar, 3-bromoisoquinoline from ABCR, isoquinolin-3-amine, tris(dibenzylideneacetone)dipalladium(0), 1,3-bis(diphenylphosphino)propane, and 2-(methylthio)ethanol from Sigma Aldrich, and potassium tert-butoxide from Acros Organics. [**1**]$(PF_6)_2$ was synthesized according to literature.[6] All metal complexes were synthesized in dim light and stored in darkness. All reactants and solvents were used without further purification. ^{1}H NMR spectra were recorded on a Bruker AV-300 spectrometer. Chemical shifts are indicated in ppm. Mass spectra were recorded by using an MSQ Plus Spectrometer.

3.4.2 Synthesis

3,3'-biisoquinoline (i-biq)

i-biq was synthesized according to literature.[21]

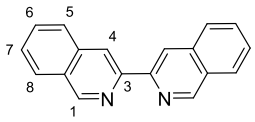

^{1}H NMR (300 MHz, chloroform-d, 298 K) δ 9.38 (s, 2H, 1), 8.93 (s, 2H, 4), 8.08 – 7.96 (m, 4H, 8 + 5), 7.74 (ddd, *J* = 8.2, 6.9, 1.3 Hz, 2H, 6), 7.63 (ddd, *J* = 8.1, 6.9, 1.2 Hz, 2H, 7). *^{13}C NMR (75 MHz, chloroform-d, 298 K)* δ 152.3 (1), 137.0 (3), 131.0 (6), 128.7 + 127.9 (4a + 8a), 127.9 + 127.8 (5 + 8), 127.8 (7), 118.1 (4). *ES MS m/z (calc.):* 257.3 (257.1 $[M + H]^+$).

di(isoquinolin-3-yl)amine (i-Hdiqa)

i-Hdiqa was synthesized according to literature procedures described for the synthesis of other dipyridylamine derivatives.[33]

Tris(dibenzylideneacetone)dipalladium(0) (18 mg, 0.020 mmol) and 1,3-bis(diphenylphosphino)propane (16 mg, 0.039 mmol) were dissolved in dry toluene (25 mL). 3-Bromoisoquinoline (200 mg, 0.97 mmol), isoquinolin-3-amine (170 mg, 1.2 mmol), and potassium tert-butoxide (150 mg, 1.4 mmol) were added in this order under dinitrogen atmosphere. The resultant mixture was stirred and heated to reflux under dinitrogen atmosphere overnight at 110 °C. The solution was cooled down to room temperature and

filtered over *Celite*. The cake was washed four times with ethyl acetate (30 mL). The solvent was evaporated with a rotary evaporator using a water bath set at 40 °C. The crude product was purified by column chromatography on silica with pentane/ethyl acetate 1:1 + 0.5% triethylamine as eluent (R_f = 0.75), to yield i-Hdiqa as a yellow powder. Yield: 48% (130 mg, 0.48 mmol).

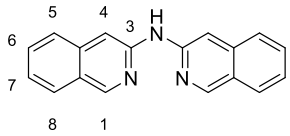

^{1}H NMR (300 MHz, chloroform-d, 298 K) δ (ppm) 9.05 (s, 2H, 1), 7.88 (dd, *J* = 8.2, 1.1 Hz, 2H, 8), 7.80 (s, 2H, 4), 7.73 (dd, *J* = 8.3, 1.1 Hz, 2H, 5), 7.64 (s, 1H, NH), 7.58 (ddd, *J* = 8.2, 6.8, 1.2 Hz, 2H, 7), 7.37 (ddd, *J* = 8.1, 6.8, 1.1 Hz, 2H, 6). *^{13}C NMR (75 MHz, chloroform-d, 298 K)* δ (ppm) 151.6 (1), 150.0 (3), 138.6 (4a), 130.7 (6), 127.9 (8), 125.8 (5), 125.2 (8a), 124.4 (7), 103.0 (4). *ES MS m/z (calc.):* 272.4 (272.1, $[M + H]^+$).

[Ru(tpy)(i-biq)(Cl)]Cl

[Ru(tpy)(Cl)$_3$] (174 mg, 0.394 mmol), i-biq (101 mg, 0.394 mmol), and lithium chloride (18.4 mg, 0.433 mmol) were dissolved in a degassed ethanol/water mixture (3:1, 32 mL). Triethylamine (0.756 mL, 0.630 mmol) was added and the reaction mixture was refluxed under dinitrogen atmosphere overnight. The reaction mixture was filtered hot over *Celite* and the cake was washed with ethanol until the filtrate was colorless. After evaporation of the solvents, the crude product was purified by column chromatography on silica with dichloromethane/methanol (9:1) as eluent (R_f = 0.64). The product was obtained as a dark brown solid. Yield: 94% (245 mg, 0.370 mmol).

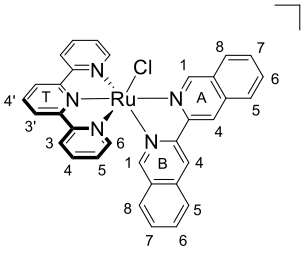

^{1}H NMR (300 MHz, methanol-d$_4$, 298 K) δ 10.79 (s, 1H, A1), 9.32 (s, 1H, A4), 9.03 (s, 1H, B4), 8.69 (d, *J* = 8.1 Hz, 2H, T3'), 8.55 (dt, *J* = 8.1, 1.2 Hz, 2H, T3), 8.44 – 8.33 (m, 2H, A5 + A8), 8.20 (t, *J* = 8.1 Hz, 1H, T4'), 8.10 – 7.82 (m, 8H, B5 + A6 + A7 + B1 + T6 + T4), 7.72 (ddd, *J* = 8.2, 6.5, 1.6 Hz, 1H, B6), 7.66 – 7.50 (m, 2H, B7 + B8), 7.28 (ddd, *J* = 7.3, 5.6, 1.4 Hz, 2H, T5). *^{13}C NMR (75 MHz, methanol-d$_4$, 298 K)* δ 160.5 + 160.0 (C_q T2 + T2'), 156.9 (A1), 156.0 (B1), 153.1 (T6), 152.6 + 151.1 (C_q A3 + B3), 138.3 (T4), 136.8 + 135.7 (C_q A4a + B4a), 135.3 (T4'), 133.7 (A6), 133.4 (B6), 131.3 (A7), 131.0 + 130.3 (C_q A8a + B8a), 130.8 (B7), 129.0 + 128.7 + 128.5 (A5 + B5 + A8), 128.4 (T5), 127.2 (B8), 124.9 (T3), 123.7 T3'), 121.4 (A4), 120.8 (B4). *ES MS m/z (calc.):* 626.6 (626.1 $[M - Cl]^+$).

[Ru(tpy)(i-Hdiqa)(Cl)]Cl

[Ru(tpy)(Cl)$_3$] (135 mg, 0.307 mmol), i-Hdiqa (100 mg, 0.369 mmol), and lithium chloride (65 mg, 1.5 mmol) were dissolved in a degassed ethanol/water mixture (3:1, 20 mL). Triethylamine (400 μL, 2.6 mmol) was added and the reaction mixture was refluxed under dinitrogen atmosphere for 4 h. The reaction mixture was filtered hot over *Celite* and the cake was washed with ethanol until the filtrate was colorless. After evaporation of the solvents, the crude product was purified by column chromatography on silica with dichloromethane/methanol (9:1) as eluent (R_f = 0.42), to yield a dark reddish brown solid. Yield: 83% (173 mg, 0.256 mmol).

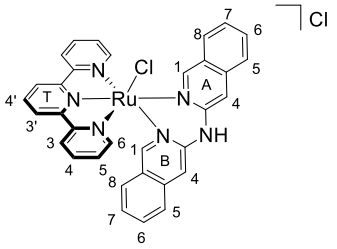

^{1}H NMR (300 MHz, methanol-d_4, 298 K) δ 10.35 (s, 1H, A1), 8.61 (d, *J* = 8.1 Hz, 2H, T3′), 8.61 – 8.56 (m, 2H, T6), 8.55 (dd, *J* = 8.0, 1.2 Hz, 2H, T3), 8.14 (dd, *J* = 8.4, 1.1 Hz, 1H, A8), 8.10 (t, *J* = 8.1 Hz, 1H, T4′), 8.03 (dd, *J* = 8.3, 1.0 Hz, 1H, A5), 8.01 (ddd, *J* = 8.0, 7.8, 1.5 Hz, 2H, T4), 7.85 (ddd, *J* = 8.3, 6.9, 1.1 Hz, 1H, A6), 7.84 (s, 1H, A4), 7.64 (ddd, *J* = 8.4, 6.9, 1.0 Hz, 1H, A7), 7.59 (dd, *J* = 8.1, 1.1 Hz, 1H, B5), 7.56 – 7.51 (m, 2H, T5), 7.50 (s, 1H, B1), 7.51 – 7.47 (m, 1H, B6), 7.31 (dd, *J* = 8.3, 1.0 Hz, 1H, B8), 7.23 (s, 1H, B4), 7.23 (ddd, *J* = 8.3, 6.6, 1.1 Hz, 1H, B7). *^{13}C NMR (75 MHz, methanol-d_4, 298 K)* δ 160.8 + 160.8 (C_q T2 + T2′), 160.1 (A1), 154.6 (T6), 154.4 (B1), 151.3 (C_q A3 or B3), 139.6 (C_q A4a or B4a), 138.4 (T4), 135.2 (T4′), 133.6 (A6), 133.4 (B6), 128.8 (A8), 128.3 (T5), 127.9 + 126.9 (C_q A8a + B8a), 127.7 (A7), 127.4 (B7), 127.1 (B8), 126.8 (A5), 126.2 (B5), 124.9 (T3), 123.7 (T3′), 108.0 (A4), 107.3 (B4), two quaternary carbons are missing: C_q A3 or B3, C_q A4a or B4a. *ES MS m/z (calc.):* 641.6 (641.1 [M – Cl]$^+$).

[Ru(tpy)(i-biq)(Hmte)](PF$_6$)$_2$, [2](PF$_6$)$_2$

[Ru(tpy)(i-biq)(Cl)]Cl (21 mg, 0.032 mmol) and $AgPF_6$ (17 mg, 0.067 mmol) were dissolved in a degassed acetone/water mixture (3:5, 16 mL). 2-(Methylthio)ethanol (138 μL, 1.53 mmol) was added in excess to the reaction mixture. The reaction was stirred and heated to reflux under dinitrogen atmosphere for 4 h, filtered hot over *Celite*, and the cake was washed with acetone until the filtrate was colorless. The solvents were removed by rotary evaporation. The product was dissolved in a minimum amount of acetone and reprecipitated by addition to an excess of diethyl ether. Filtration yielded the final product, which was dried in air and then under vacuum as a bright orange powder. Yield: 48% (15 mg, 0.015 mmol).

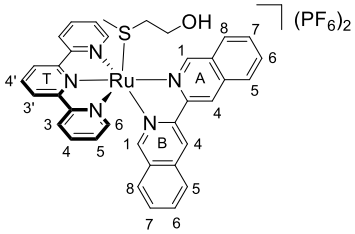

^{1}H NMR (300 MHz, acetone-d_6, 298 K) δ (ppm) 10.64 (s, 1H, A1), 9.54 (s, 1H, A4), 9.32 (s, 1H, B4), 8.99 (d, *J* = 8.1 Hz, 2H, T3′), 8.79 (dd, *J* = 8.0, 1.3 Hz, 2H, T3), 8.57 (t, *J* = 8.1 Hz, 1H, T4′), 8.54 (d, *J* = 8.3 Hz, 2H, A8), 8.42 (d, *J* = 8.2 Hz, 1H, A5), 8.27 – 8.22 (m, 3H, B1 + T6), 8.17 – 8.09 (m, 4H, T4 + B5 + A6), 8.04 (ddd, *J* = 8.2, 7.0, 1.2 Hz, 1H, A7), 7.84 (ddd, *J* = 8.2, 6.7, 1.4 Hz, 1H, B6), 7.71 (d, *J* = 8.0 Hz, 1H, B8), 7.63 (ddd, *J* = 8.2, 6.7, 1.0 Hz, 1H, B7), 7.47 (ddd, *J* = 7.7, 5.5, 1.3 Hz, 2H, T5), 4.77 (t, *J* = 4.7 Hz, 1H, O<u>H</u>), 3.59 (dt, *J* = 5.0, 4.7 Hz, 2H, S-CH$_2$-C<u>H$_2$</u>), 2.10 (t, *J* = 5.0 Hz, 2H, S-C<u>H$_2$</u>), 1.54 (s, 3H, S-C<u>H$_3$</u>). *^{13}C NMR (300 MHz, acetone-d_6, 298 K)* δ (ppm) 159.2 + 158.8 (C_q T2 + T2′), 156.8 (A1), 154.7 (B1), 154.4 (T6), 150.8 + 150.4 (C_q A3 + B3), 139.7 (T4), 137.7 (T4′), 136.7 + 136.1 (C_q A4a + B4a), 134.0 (B6 + A6), 131.1 (A7), 130.8 + 129.8 (C_q A8a + B8a), 130.6 (B7), 129.3 (T5), 129.1 (A8), 128.7 (A5), 128.3 (B5 + B8), 126.0 (T3), 125.3 (T3′), 122.1 (A4), 121.4 (B4), 58.8 (S-CH$_2$-<u>C</u>H$_2$), 38.4 (S-<u>C</u>H$_2$), 14.8 (S-<u>C</u>H$_3$). *High resolution ES MS m/z (calc.):* 341.5644 (341.5645, [M – 2PF$_6$]$^{2+}$). *Elem. Anal. Calc. for $C_{36}H_{31}F_{12}N_5OP_2RuS$:* C, 44.45; H, 3.21; N, 7.20. *Found:* C, 43.75; H, 3.30; N, 7.12.

[Ru(tpy)(i-Hdiqa)(Hmte)](PF$_6$)$_2$, [3](PF$_6$)$_2$

[Ru(tpy)(i-Hdiqa)(Cl)]Cl (150 mg, 0.222 mmol) and $AgPF_6$ (123 mg, 0.488 mmol) were dissolved in a degassed acetone/water mixture (3:5, 30 mL). 2-(Methylthio)ethanol (1 mL, 0.01 mol) was added in excess to the reaction mixture. The reaction was stirred and heated to reflux under dinitrogen atmosphere for 3 h, filtered hot over *Celite*, and the cake was washed with acetone until the filtrate was colorless. The solvents were removed by rotary evaporation. The product was dissolved in a minimum amount of

acetone and precipitated by addition to an excess of diethyl ether. Filtration yielded the final product as an orange powder, which was dried in air and then under vacuum. Yield: 60% (132 mg, 0.134 mmol).

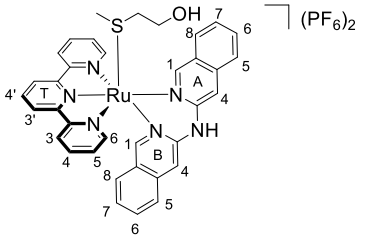

^{1}H NMR (300 MHz, acetone-d_6, 298 K) δ (ppm) 10.15 (s, 1H, A1), 10.01 (s, 1H, NH), 8.95 (dd, *J* = 5.6, 0.8 Hz, 2H, T6), 8.89 (d, *J* = 8.2 Hz, 2H, T3'), 8.77 (dd, *J* = 8.1, 0.7 Hz, 2H, T3), 8.46 (t, *J* = 8.2 Hz, 1H, T4'), 8.35 (d, *J* = 8.3 Hz, 1H, A8), 8.27 (ddd, *J* = 8.1, 7.8, 0.8 Hz, 2H, T4), 8.15 (s, 1H, A4), 8.10 (d, *J* = 8.4 Hz 1H, A5), 7.93 (ddd, *J* = 8.3, 6.8, 1.2 Hz, 1H, A6), 7.79 (s, 1H, B1), 7.78 – 7.68 (m, 4H, T5 + A7 + B5), 7.65 – 7.58 (m, 2H, B4 + B6), 7.48 (d, *J* = 8.3 Hz, 1H, B8), 7.30 (ddd, *J* = 8.3, 6.7, 0.9 Hz, 1H, B7), 4.13 (t, *J* = 5.2 Hz, 1H, -OH), 3.49 (dt, *J* = 5.6, 5.2 Hz, 2H, S-CH_2-CH_2), 1.91 (t, *J* = 5.6 Hz, 2H, S-CH_2), 1.37 (s, 3H, S-CH_3). *^{13}C NMR (300 MHz, acetone-d_6, 298 K)* δ (ppm) 159.4 + 159.3 (C_q T2 + T2'), 159.0 (A1), 155.7 (T6), 152.7 (B1), 151.4 + 151.0 (C_q A3 + B3), 139.8 (T4), 139.4 + 138.6 (C_q A4a + B4a), 137.4 (T4'), 133.9 (A6), 133.9 (B6), 129.1 (T5), 128.9 (A8), 128.2 + 126.7 (C_q A8a + B8a), 128.1 (B8), 127.8 (A7), 127.3 (B7), 126.7 (A5), 126.1 (B5), 126.0 (T3), 125.3 (T3'), 110.2 (A4), 108.7 (B4), 59.0 (S-CH_2-CH_2), 38.0 (S-CH_2), 15.1 (S-CH_3). *High resolution ES MS m/z (calc.):* 349.0698 (349.0699, $[M - 2PF_6]^{2+}$). *Elem. Anal. Calc. for $C_{36}H_{32}F_{12}N_6OP_2RuS$ + 3 H_2O:* C, 41.51; H, 3.68; N, 8.07. *Found:* C, 41.77; H, 3.45; N, 8.11.

3.4.3 Single Crystal X-Ray crystallography

Single crystals of [**2**]$(PF_6)_2$ were obtained by recrystallization through liquid-vapor diffusion using acetonitrile as solvent and diisopropyl ether as counter-solvent. In short, 1 mg of [**2**]$(PF_6)_2$ was dissolved in acetonitrile (1 mL) and placed in a small vial. This vial was placed in a larger vial containing diisopropyl ether (2.8 mL). The large vial was closed and vapor diffusion within a few days afforded X-ray quality crystals.

All reflection intensities were measured at 110(2) K using a SuperNova diffractometer (equipped with Atlas detector) with Cu *Kα* radiation (*λ* = 1.54178 Å) under the program CrysAlisPro (Version CrysAlisPro 1.171.39.29c, Rigaku OD, 2017). The same program was used to refine the cell dimensions and for data reduction. The structure was solved with the program SHELXS-2014/7 (Sheldrick, 2015) and was refined on F^2 with SHELXL-2014/7 (Sheldrick, 2015). Analytical numeric absorption correction using a multifaceted crystal model was applied using CrysAlisPro. The temperature of the data collection was controlled using the system Cryojet (manufactured by Oxford Instruments). The H atoms were placed at calculated positions using the instructions AFIX 23, AFIX 43 or AFIX 137 with isotropic displacement parameters having values 1.2 or 1.5 *U*eq of the attached C atoms. The H atoms attached to the disordered hydroxyl groups O1A/O1A' and O1B/O1B' could not be retrieved reliably from difference Fourier maps, and no AFIX 147 was used because of the disorder. The crystal refines in the space group *Pca*2$_1$ and is racemically twinned. The Flack parameter refines to 0.539(16).

The structure of [**2**]$(PF_6)_2$ is significantly disordered. Two of the four crystallographically independent counter ions were found to be disordered over (at least) 3 different orientations. The terpyridine ligand on one of the two ruthenium complexes is disordered over two orientations. The hydroxyl groups of the Hmte ligands for both Ru1 and Ru2 complexes are disordered over two orientations. [**2**]$(PF_6)_2$: 0.51 × 0.10 × 0.05 mm^3, Orthorhombic, *Pca*2$_1$, a = 22.0959 (11), b = 8.8289 (2), c = 37.3521 (9) Å, V = 7286.7 (4) Å^3, Z = 8, μ = 5.78 mm^{-1}, transmission factor range: 0.280–0.812. 23674 Reflections were measured up to a resolution of (sin θ/λ)max = 0.616 Å^{-1}. 11592 Reflections were unique (R_{int} = 0.037), of which 10905

were observed [I > 2σ(I)]. 1423 Parameters were refined. R1/wR2 [I > 2σ(I)]: 0.0525/ 0.1383. R1/wR2 [all refl.]: 0.0558/ 0.1407. S= 1.11. Residual electron density found between −0.87 and 1.63 e Å^{-3}.

3.4.4 DFT calculations

DFT was used to perform electronic structure calculations. The structure of [**2**]$^{2+}$ and [**3**]$^{2+}$ was optimized using ADF from SCM,[34] using the PBE0 hybrid functional, a triple zeta basis set (TZP) for all atoms, and COSMO to simulate solvent effects in water.

3.4.5 Irradiation experiments monitored with UV-vis and MS

Photoreactions monitored with UV-vis spectroscopy were performed on a Cary Varian spectrometer equipped with temperature control set to 310 K and a magnetic stirrer. The measurements were performed in a quartz cuvette, containing 3 mL of solution. The stirred sample was irradiated perpendicularly to the axis of the spectrometer with the beam of an LED fitted to the top of the cuvette.

For photoactivation with green light, an LED light source (λ = 517 nm, $\Delta\lambda_{1/2}$ = 23 nm, 5.2 mW) was used, an absorption spectrum was measured every 30 sec for 70 min for [**2**](PF$_6$)$_2$ and 47 min for [**3**](PF$_6$)$_2$. [Ru] = 0.074 and 0.061 mM and $\Phi = 5.2 \cdot 10^{-8}$ mol $\cdot$ s^{-1} for [**2**](PF$_6$)$_2$ and [**3**](PF$_6$)$_2$. Data were analyzed using Microsoft Excel. Mass spectrometry was performed at the beginning and at the end of the irradiation to confirm the nature of the reagent and products. Photosubstitution quantum yield calculations were performed using the Glotaran Software package as described in Appendix I. The conditions are summarized in Table AIII.1.

3.4.6 Cytotoxicity and cellular uptake

Cytotoxicity assays and cellular uptake experiments were performed using the protocols described in Appendix I.

3.4.7 Supporting information

DFT models, dark stability measurements, determination of molar extinction coefficients, singlet oxygen production and phosphorescence spectra, photosubstitution conditions, and light dose determinations for [**2**](PF$_6$)$_2$ and [**3**](PF$_6$)$_2$ are provided in Appendix III.

3.5 Contribution

Ingrid Flashpohler helped performing cytotoxicity tests, Dr. Claudia Schmidt and Prof. Ingo Ott performed HRCS-AAS measurements for cell uptake, Xuequan Zhou performed singlet oxygen measurements, Dr. Vincent van Rixel grew single crystals, and Dr. Maxime Siegler performed X-ray diffraction experiments and crystal structure determination. Dr. Sylvestre Bonnet performed DFT studies and, together with Prof. Lies Bouwman, he provided experimental guidance and significant editorial feedback.

3.6 References

1 L. Zayat, O. Filevich, L. M. Baraldo, and R. Etchenique, *Philos. Trans. Royal Soc. A* **2013**, 371 (1995), 20120330.

2 A. Li, C. Turro, and J. J. Kodanko, *Chem. Commun.* **2018**, 54 (11), 1280-1290.

3 J. Wei and A. K. Renfrew, *J. Inorg. Biochem.* **2018**, 179 (-), 146-153.

4 H. Chan, J. B. Ghrayche, J. Wei, and A. K. Renfrew, *Eur. J. Inorg. Chem.* **2017**, 2017 (12), 1679-1686.

5 U. Basu, J. Karges, F. Chotard, C. Balan, P. Le Gendre, G. Gasser, E. Bodio, and R. Malacea Kabbara, *Polyhedron* **2019**, doi.org/10.1016/j.poly.2019.02.041.

6 A. Bahreman, B. Limburg, M. A. Siegler, E. Bouwman, and S. Bonnet, *Inorg. Chem.* **2013**, 52 (16), 9456-69.

7 O. Novakova, J. Kasparkova, O. Vrana, P. M. van Vliet, J. Reedijk, and V. Brabec, *Biochemistry* **1995**, 34 (38), 12369-12378.

8 E. Alessio, *Eur. J. Inorg. Chem.* **2017**, 2017 (12), 1549-1560.

9 L. N. Lameijer, C. van de Griend, S. L. Hopkins, A.-G. Volbeda, S. H. C. Askes, M. A. Siegler, and S. Bonnet, *J. Am. Chem. Soc.* **2019**, 141 (1), 352-362.

10 H. Huang, P. Zhang, H. Chen, L. Ji, and H. Chao, *Chem. Eur. J.* **2015**, 21 (2), 715-725.

11 U. Schatzschneider, J. Niesel, I. Ott, R. Gust, H. Alborzinia, and S. Wölfl, *ChemMedChem* **2008**, 3 (7), 1104-1109.

12 J.-A. Cuello-Garibo, C. C. James, M. A. Siegler, and S. Bonnet, *Chem. Sq* **2017**, 1 (2), 1-19.

13 B. Siewert, V. H. van Rixel, E. J. van Rooden, S. L. Hopkins, M. J. Moester, F. Ariese, M. A. Siegler, and S. Bonnet, *Chem.Eur. J.* **2016**, 22 (31), 10960-10968.

14 B. S. Howerton, D. K. Heidary, and E. C. Glazer, *J. Am. Chem. Soc.* **2012**, 134 (20), 8324-8327.

15 L. Kohler, L. Nease, P. Vo, J. Garofolo, D. K. Heidary, R. P. Thummel, and E. C. Glazer, *Inorg. Chem.* **2017**, 56 (20), 12214-12223.

16 L. N. Lameijer, D. Ernst, S. L. Hopkins, M. S. Meijer, S. H. Askes, S. E. Le Dévédec, and S. Bonnet, *Angew. Chem., Int. Ed.* **2017**, 56 (38), 11549-11553.

17 A. C. Komor, C. J. Schneider, A. G. Weidmann, and J. K. Barton, *J. Am. Chem. Soc.* **2012**, 134 (46), 19223-19233.

18 V. H. S. van Rixel, B. Siewert, S. L. Hopkins, S. H. C. Askes, A. Busemann, M. A. Siegler, and S. Bonnet, *Chem. Sci.* **2016**, 7 (8), 4922-4929.

19 L. N. Lameijer, T. G. Brevé, V. H. S. van Rixel, S. H. C. Askes, M. A. Siegler, and S. Bonnet, *Chem. Eur. J.* **2018**, 24 (11), 2709-2717.

20 W. Han Ang and P. J. Dyson, *Eur. J. Inorg. Chem.* **2006**, 2006 (20), 4003-4018.

21 T. Funayama, M. Kato, H. Kosugi, M. Yagi, J. Higuchi, and S. Yamauchi, *Bull. Chem. Soc. Jpn.* **2000**, 73 (7), 1541-1550.

22 M. Toyama, R. Suganoya, D. Tsuduura, and N. Nagao, *Bull. Chem. Soc. Jpn.* **2007**, 80 (5), 922-936.

23 N. Chanda, S. M. Mobin, V. G. Puranik, A. Datta, M. Niemeyer, and G. K. Lahiri, *Inorg. Chem.* **2004**, 43 (3), 1056-1064.

24 K. Robinson, G. V. Gibbs, and P. H. Ribbe, *Science* **1971**, 172 (3983), 567-570.

25 M. E. Fleet, *Mineral. Mag.* **1976**, 40 (313), 531-533.

26 D. Garcìa-Fresnadillo, Y. Georgiadou, G. Orellana, A. M. Braun, and E. Oliveros, *Helv. Chim. Acta* **1996**, 79 (4), 1222-1238.

27 R. E. Goldbach, I. Rodriguez-Garcia, J. H. van Lenthe, M. A. Siegler, and S. Bonnet, *Chem.Eur. J.* **2011**, 17 (36), 9924-9929.

28 B. Siewert, M. Langerman, Y. Hontani, J. T. M. Kennis, V. H. S. van Rixel, B. Limburg, M. A. Siegler, V. Talens Saez, R. E. Kieltyka, and S. Bonnet, *Chem. Commun.* **2017**, 53 (81), 11126-11129.

29 J. Snellenburg, J., S. Laptenok, R. Seger, K. Mullen, M., and I. Van Stokkum, H.M., *J. Stat. Softw.* **2012**, 49 (3), 1-22.

30 S. Hopkins, B. Siewert, S. Askes, P. Veldhuizen, R. Zwier, M. Heger, and S. Bonnet, *Photochem. Photobiol. Sci.* **2016**, 15 (5), 644-653.

31 J.-A. Cuello-Garibo, M. S. Meijer, and S. Bonnet, *Chem. Commun.* **2017**, 53 (50), 6768-6771.
32 D. F. Azar, H. Audi, S. Farhat, M. El-Sibai, R. J. Abi-Habib, and R. S. Khnayzer, *Dalton Trans.* **2017**, 46 (35), 11529-11532.
33 R. Marion, F. Sguerra, F. Di Meo, E. Sauvageot, J.-F. Lohier, R. Daniellou, J.-L. Renaud, M. Linares, M. Hamel, and S. Gaillard, *Inorg. Chem.* **2014**, 53 (17), 9181-9191.
34 G. te Velde, F. M. Bickelhaupt, E. J. Baerends, C. Fonseca Guerra, S. J. A. van Gisbergen, J. G. Snijders, and T. Ziegler, *J. Comput. Chem.* **2001**, 22 (9), 931-967.